Creep Deformation of Sn-3.5Ag-xCu and Sn-3.5Ag-xBi Solder Joints

S.W. SHIN[1,2] and JIN YU[1]

1.—Center for Electronic Packaging Materials, Korea Advanced Institute of Science and Technology, Daejon, 305-701 Korea. 2.—E-mail: swshin@kaist.ac.kr

Creep properties of lead-free Sn-3.5Ag-based alloys with varying amounts of Cu or Bi were studied by single lap-shear test. Solder balls with five different compositions of Cu (0 wt.%, 0.75 wt.%, 1.5 wt.%) and Bi (2.5 wt.%, 7.5 wt.%) were reflowed on Cu. The Cu-containing alloy had a lower creep rate than the Bi-containing alloy. The Sn-3.5Ag alloy showed the lowest creep rate on Cu, implying that the Cu element already dissolved in the Sn-3.5Ag alloy during reflow. The Cu-containing alloy was strengthened by dispersed small precipitates of Cu_6Sn_5. As the Cu content increased up to 1.5 wt.%, the Cu_6Sn_5 coarsened and platelike Ag_3Sn intermetallics were found, which deteriorated the creep resistance.

Key words: Creep, lead-free solders, lap shear

INTRODUCTION

Eutectic Sn-Pb has been used as a solder alloy in microelectronic packages because of its good mechanical and electrical properties. Environmental protection, however, has encouraged worldwide legislative actions to ban Pb in electronic devices. Research on Pb-free alloys has focused on binary alloy systems.[1–3] One of the most promising alloys is eutectic Sn-3.5Ag, which has good creep and thermal fatigue resistance, but a relatively high melting point and poor wettability, which require ternary elements, such as Cu, Bi, In, or Zn.[4] Recently, the mechanical properties and the interfacial reactions of the ternary alloys have been extensively studied. Most mechanical studies, however, have been done with the alloy itself, not with the real package structure, because of the difficulty of performing the experiment.

Generally, thermal fatigue is induced on the solder joints from the thermal mismatch between chip and substrate combined with cyclic changes of temperature in microelectronic devices. The difference between the highest and the lowest temperatures during operation depends on the microelectronic device itself or the environment. Because of the high homologous temperature of the solder alloy, this low-cycle fatigue induces creep-fatigue interaction of the solder. The creep characteristics are very important for reliability in microelectronics packaging. Creep results of lead-free solders have been reported, but the microstructure of bulk specimens differs from that of a solder joint. Therefore, the data of bulk creep might not be appropriate for the alloy design of solder bumps. In contrast, lap-shear creep has a similar structure to solder bumps in real packages. There are several reports on the single and double lap-shear tests from Lawrence Berkeley Laboratory.[5–7] Mei[6] showed that the stress exponent, n, was equal to 2 for 60Sn/40Pb, which was in good agreement with previous work.[8] For the Sn-3.5Ag alloy,[9] n was 5.5, similar to the result in Mathew's bulk data,[10] n = 5.0. Also, the trial to extract steady-state creep strain rates from the displacement dependent on time in fatigue test was reported.[11]

In this research, Sn-3.5Ag-xCu, -xBi solders on a Cu pad were studied with varying compositions of Cu and Bi by lap-shear test. Also, the effect of Cu dissolution from the substrate was investigated.

EXPERIMENTAL PROCEDURES

Compositions of Sn-3.5Ag-xCu and Sn-3.5Ag-xBi alloys studied are listed in Table I. The nominal compositions of Cu and Bi in the alloys were 0 wt.%, 0.75 wt.%, and 1.5 wt.%, and 2.5 wt.% and 7.5 wt.%,

(Received February 18, 2004; accepted November 1, 2004)

Table I. Composition of Solder Alloy (Wt.%)

Alloy	Sn	Ag	Bi	Cu
0Cu	95.7	3.61	—	—
0.75Cu	95.1	3.65	—	0.75
1.5Cu	94.6	3.49	—	1.48
2.5Bi	93.7	3.57	2.51	—
7.5Bi	88.5	3.63	7.62	—

respectively. After rolling the bulk solder alloy into the sheet of 0.13-mm thickness, the sheet was punched into disks with 1.5-mm diameter. The disks of the solder alloy were dropped through a vertical quartz tube filled with silicone oil from 300°C to room temperature.[12] The diameter of the solder ball was 760 μm. The balls were placed and reflowed onto the Cu pads on a FR-4 printed circuit board (PCB) of 3.2-mm thickness, as shown in Fig. 1a. The opening of Cu was 730 μm, and the other area was covered with a passivation layer. There were no other metals on the exposed Cu. The upper PCB in Fig. 1b was aligned and joined onto the PCB shown in Fig.1a. The cross-sectioned view of final test vehicle is shown in Fig. 1c. The average height of the solder joint was 0.39 mm, and all joints were within ±0.01 mm. The reflow profile is shown in Fig. 2. The specimen reflowed for 210 sec above 221°C with a peak temperature of 256°C in a hot-air convection reflow oven with a rosin mildly activated flux. To prevent the oxidation, the specimen was immersed in a silicone oil bath during the creep test. A schematic diagram of the lap-shear creep machine is shown in Fig. 3. Loads were between 5 MPa and 11 MPa. The temperature was held at 100°C, and displacement was measured with a linear variable-differential transformer.

To observe the cross-sectional view of the solder bumps, an etching solution of 25-mL distilled H_2O, 5-mL HCl with concentration 37%, and 5 g of NH_4NO_3 was used.[6] The phases at the interface were identified by energy dispersive x-ray spectroscopy, and the distribution of each element in the solder matrix was examined by an electron-probe microanalyzer (EPMA). For the microhardness test, a Vickers indenter was used after polishing the specimen with 1-μm alumina powder. A load of 10 g was applied, and the eight

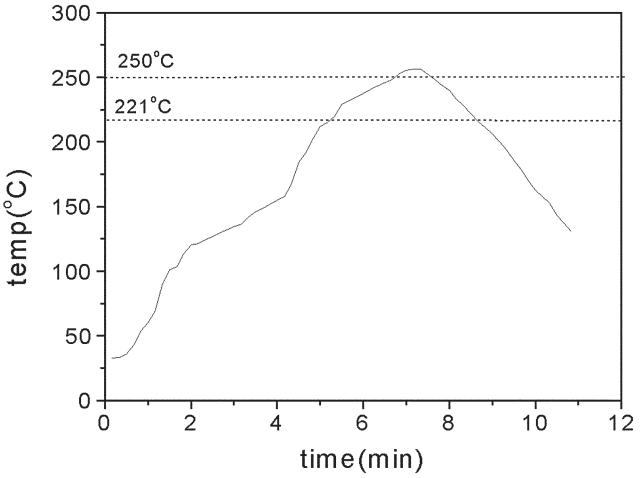

Fig. 2. A reflow profile of the specimen.

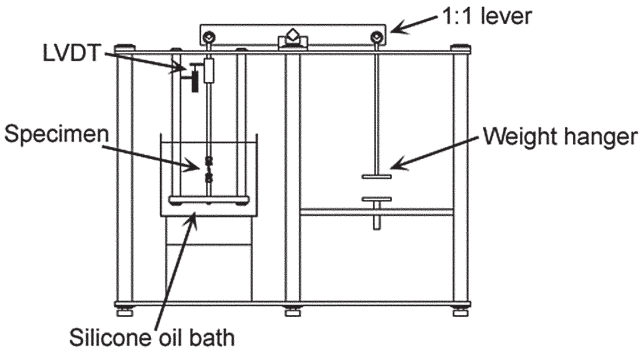

Fig. 3. The schematic side view of the lap-shear creep machine.

indentation values were measured from the two solder joints. The indenting areas for the interface were 30–40 μm away from the Cu pad. For transmission electron microscopy (TEM) analysis, the specimen was sliced cross sectionally by a diamond saw and polished to 50 μm by sandpaper. The specimen was ground to 10 μm by a dimpler and then attached to a 3-mm TEM grid. Finally, thin foil was prepared by an Ar ion miller, and the TEM image was observed with a model JEM-3010 from Japan Electron Optics Ltd. (JEOL, Tokyo).

RESULTS AND DISCUSSION

Figure 4 shows typical creep curves of Sn-3.5Ag specimens on Cu at various loads. The shear strain

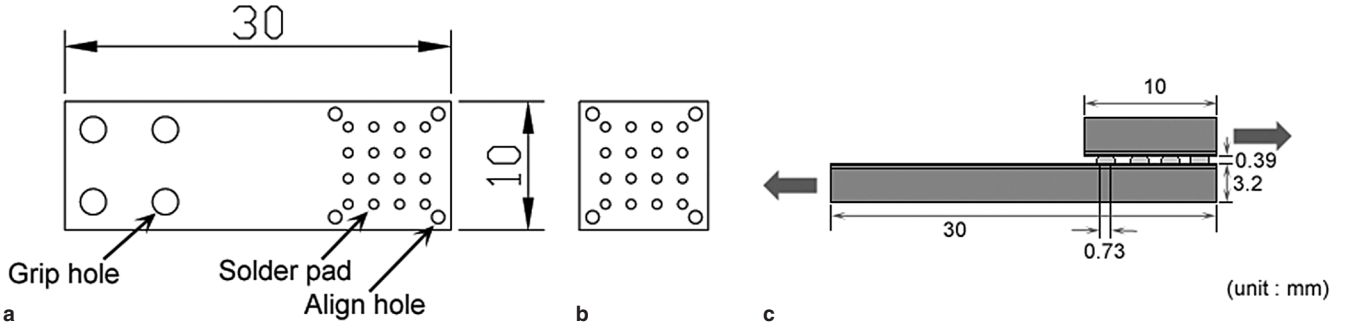

Fig. 1. The dimension of a lap-shear creep specimen (in mm): (a) lower part and (b) upper part. (c) Cross-sectional view of lap-shear creep specimen.

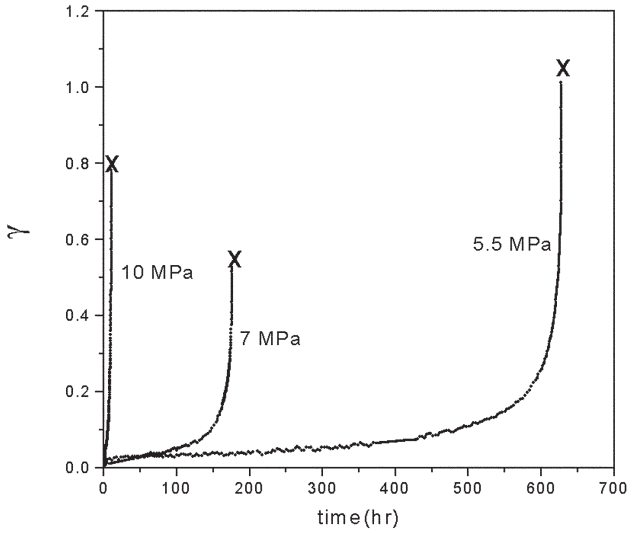

Fig. 4. Lap-shear creep curve in the Sn-3.5Ag alloy on the Cu pad in a variation of loads.

(γ) is defined as the shear displacement over the solder joint height. After primary creep of a few hours, a long steady-state creep region was followed by tertiary creep. Unlike the rupture appearance of the bulk specimen by necking,[13] an abrupt tertiary creep region was found in the creep curve.

Figure 5 shows the minimum shear-strain rates of the lap-shear test as a function of applied stress. Generally, the steady-state creep rate above $0.5T_m$ is expressed as Dorn's equation:

$$\dot{\varepsilon}_s = \frac{ADGb}{kT}\left(\frac{\sigma}{G}\right)^n$$

where $D = D_o \exp(-Q/RT)$. Here, D is a diffusion coefficient, G is the shear modulus, b is Burger's vector, k is Boltzmann's constant, A is a constant, and n is the stress exponent. Or more simply represented by Norton's power-law equation:

$$\dot{\varepsilon}_s = B\sigma^n$$

where B is a constant.

In this experiment, the applied load concentrated on the interface between the solder and Cu pad, and the deformation occurred mostly in the local area near the joint interface. Therefore, lap-shear strain rates were underestimated by the shear-strain definition. In previous research of the bulk creep test,[14] the Sn-3.5Ag-0.75Cu alloy showed the lowest creep strain rates. In this study, the Sn-3.5Ag alloy showed the lowest creep strain rates in the relatively lower stress range because of the strengthening effect of intermetallic compound (IMC) particles from the dissolution of the Cu pad. These dispersed IMCs could play a role in forming effective obstacles to dislocation movement. In the strengthening mechanism, there is a threshold stress that results in no strain and causes a large stress exponent as the applied stress goes down.[15,16] It appears that these fine particles do not act as effective obstacles on a high stress region in which the matrix deformation was dominant and resulted in high creep strain rates.

The Cu solubility in the liquid Sn-3.5Ag alloy was reported as 1.5 wt.%[12] so that the 0.75Cu alloy contains more than 0.75wt.%Cu. The 0.75Cu alloy showed a contrary trend compared to the 0Cu alloy because of the coarse Cu_6Sn_5 IMCs and platelike Ag_3Sn IMCs that came from the solidification of the hypereutectic alloy. In the high stress range, these second phases could bring high resistance of deformation as a role of composite material, but in the low stress range, these could bring interphase boundary slidings caused by the high energy of interphases. Therefore, the creep resistances followed the order of 0Cu, 0.75Cu, and 1.5Cu in the low stress range. The Bi-containing alloys showed rather higher creep strain rates than the Cu-containing alloys, which coincided with the result of bulk specimens.[17]

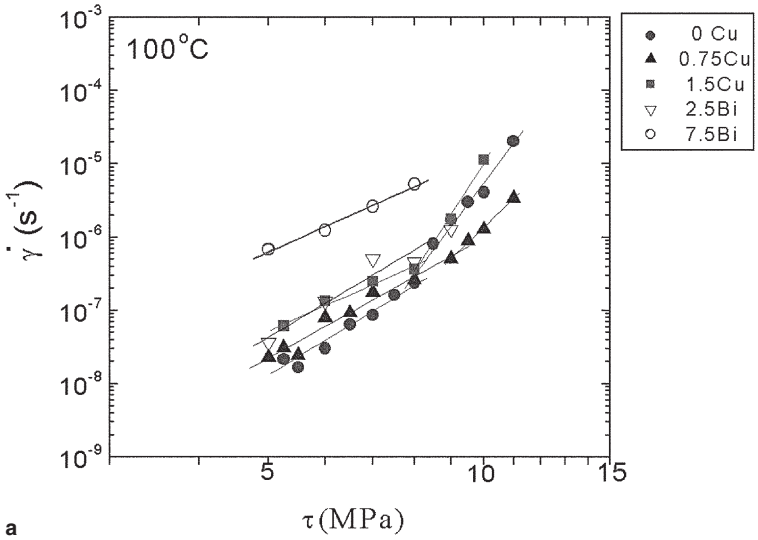

a

n	Lap shear	
	Low τ	High τ
0 Cu	6.0	13.0
0.75Cu	5.5	9.4
1.5Cu	4.4	15.3
2.5Bi	5.8	
7.5Bi	4.4	

b

Fig. 5. (a) Minimum shear-strain rates of the lap-shear creep specimen on the Cu pad at 373 K. (b) The corresponding stress exponents of each alloy.

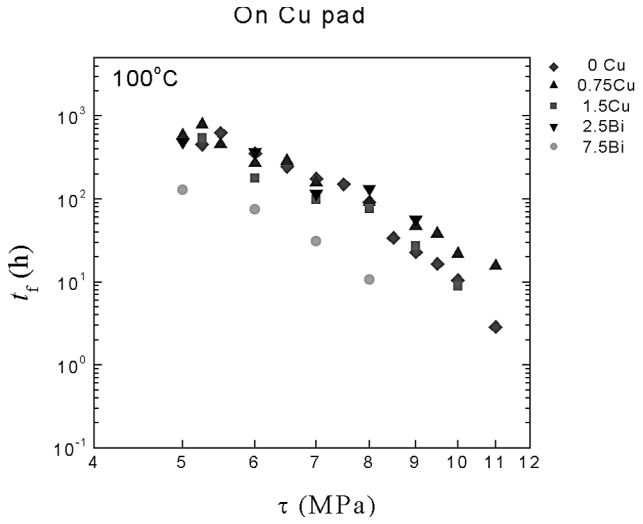

Fig. 6. Rupture times of solder alloys on the Cu pad at 373 K.

Figure 6 plots the rupture times of the solder alloys as functions of the applied stress. There was no large difference between 0Cu and 0.75Cu at the relatively low stress region or for the 2.5Bi. The rupture times of the lap-shear specimens depends on the displacement of the solder joint. Differences of rupture times are hard to distinguish. The 1.5Cu and 7.5Bi alloys have rather brittle fracture locus,[13,17] showing poor rupture times. In the case of the Cu-containing alloy, the crack propagated mostly through the solder matrices and partly through the interface between intermetallics on the Cu pad and solder matrices, while the Bi-containing alloy showed the fracture path mostly following the intermetallics on the Cu pad.

The initial microstructure of Cu-containing alloys on the Cu pad before and after creep test are shown in Fig. 7. Scalloplike Cu_6Sn_5 intermetallics were grown at the solder/Cu pad interfaces, which were rather coarsened when the Cu exists in solder matrices. Particles of Ag_3Sn were dispersed in the solder matrices, but plates of Ag_3Sn were often found in the solder matrices. The sizes of formed precipitates were so fine that the differences between Ag_3Sn and Cu_6Sn_5 were hard to distinguish, but generally Ag_3Sn showed finer particles than Cu_6Sn_5.

In the case of 0.75Cu and 1.5Cu alloys, rather coarse precipitates were found after the creep test,

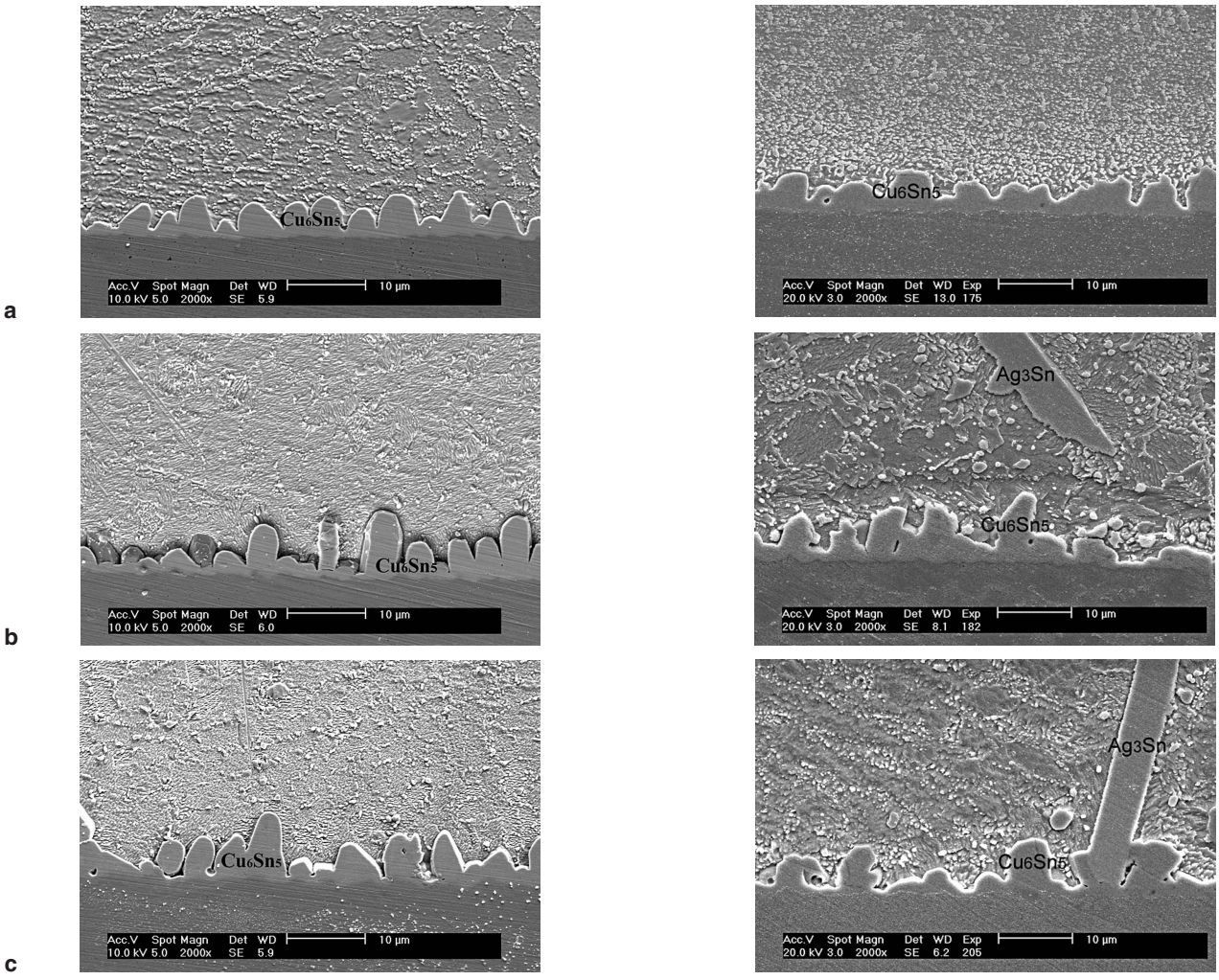

Fig. 7. The SEM images of (a) 0Cu, (b) 0.75Cu, and (c) 1.5Cu on the Cu pad before and after creep test at 7-MPa load.

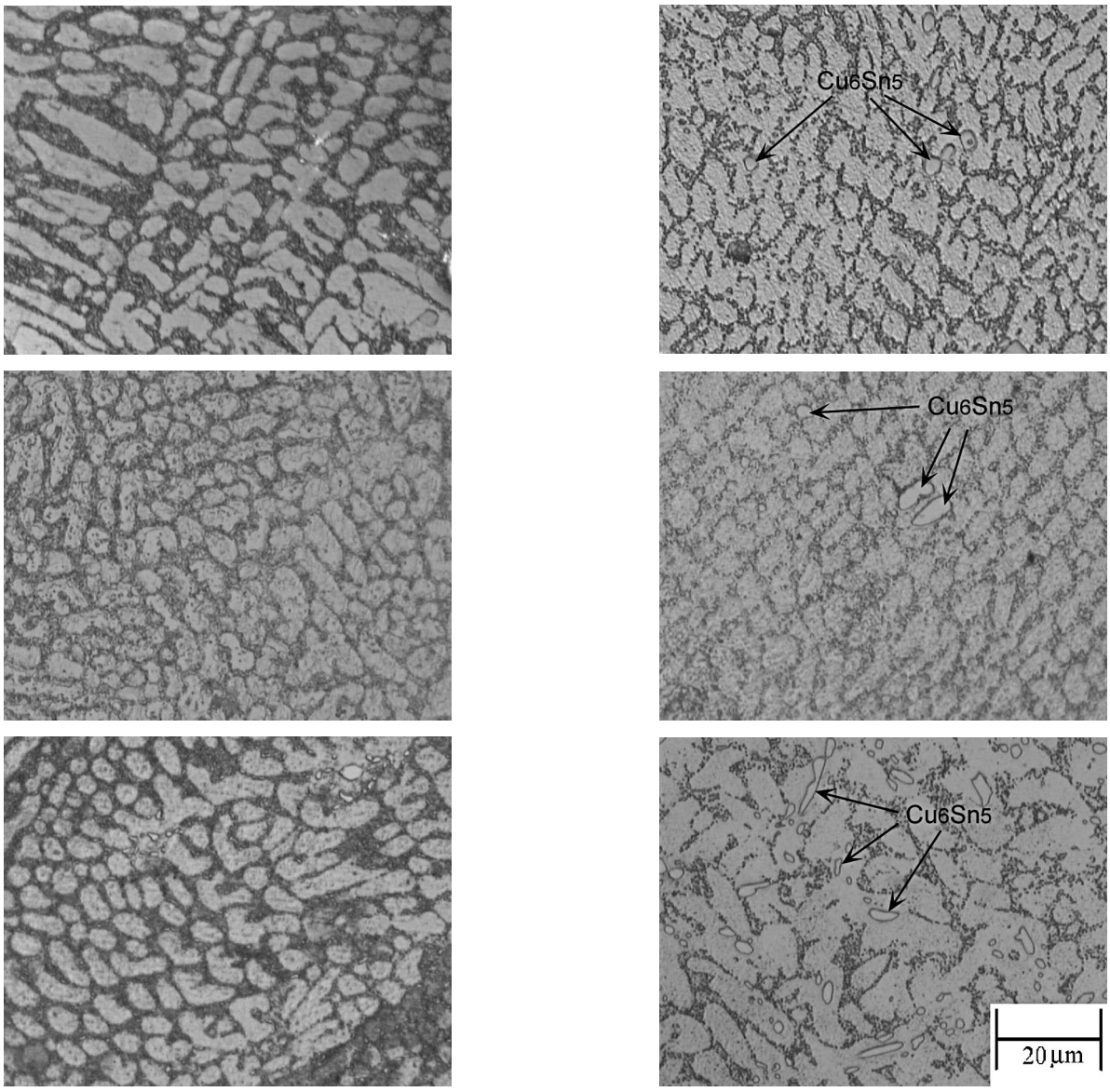

Fig. 8. Optical micrographs of the (a) 0Cu, (b) 0.75Cu, and (c) 1.5Cu solder matrix on the Cu pad before and after creep test at 6-MPa load.

as observed by optical micrograph in Fig. 8. The coarse Cu_6Sn_5 intermetallics were found just in the 1.5Cu alloy before the creep test, but all alloys showed the coarse Cu_6Sn_5 IMCs after creep test at 6 MPa. As the Cu content increased, the number of coarse Cu_6Sn_5 IMCs also increased. Generally, to contribute to the creep resistance, the particles must be stable against coalescence that their dimensions or spacings increase very slowly during creep.[18] Therefore, it is interpreted that coarsened Cu_6Sn_5 IMCs in the 1.5Cu alloy brought the lower creep resistances. By Ostwald ripening, coarsening can be minimized by low interfacial energy, low solubility, and low mobility of the strengthening phase in the matrix.[19]

Figure 9 shows element mapping by EPMA before the creep test. Most of the intermetallics have grown during the reflow time because of its rapid reaction. In the case of the 0Cu alloy on the Cu pad, the Cu element already dissolved and distributed around the β-Sn grains after reflow. The proper distribution of precipitation brought the increase of the threshold stress and resulted in the increase of the stress exponent.[20]

Vicker's hardness tests were performed to obtain the relevance between precipitates and hardness and are shown in Fig. 10. Each test was performed at the upper solder/pad interface, solder interior, and downward interface. The solder balls were also indented for reference. In the case of the 0Cu alloy, the hardness of the solder joints was higher than that of the solder balls, implying that Cu dissolution occurred from the Cu pad. For the Cu-containing alloys over 0.75 wt.%, there were no large differences in hardness. From this plot, the dissolution of Cu was verified, and there was no relation between the hardness and the creep resistance.

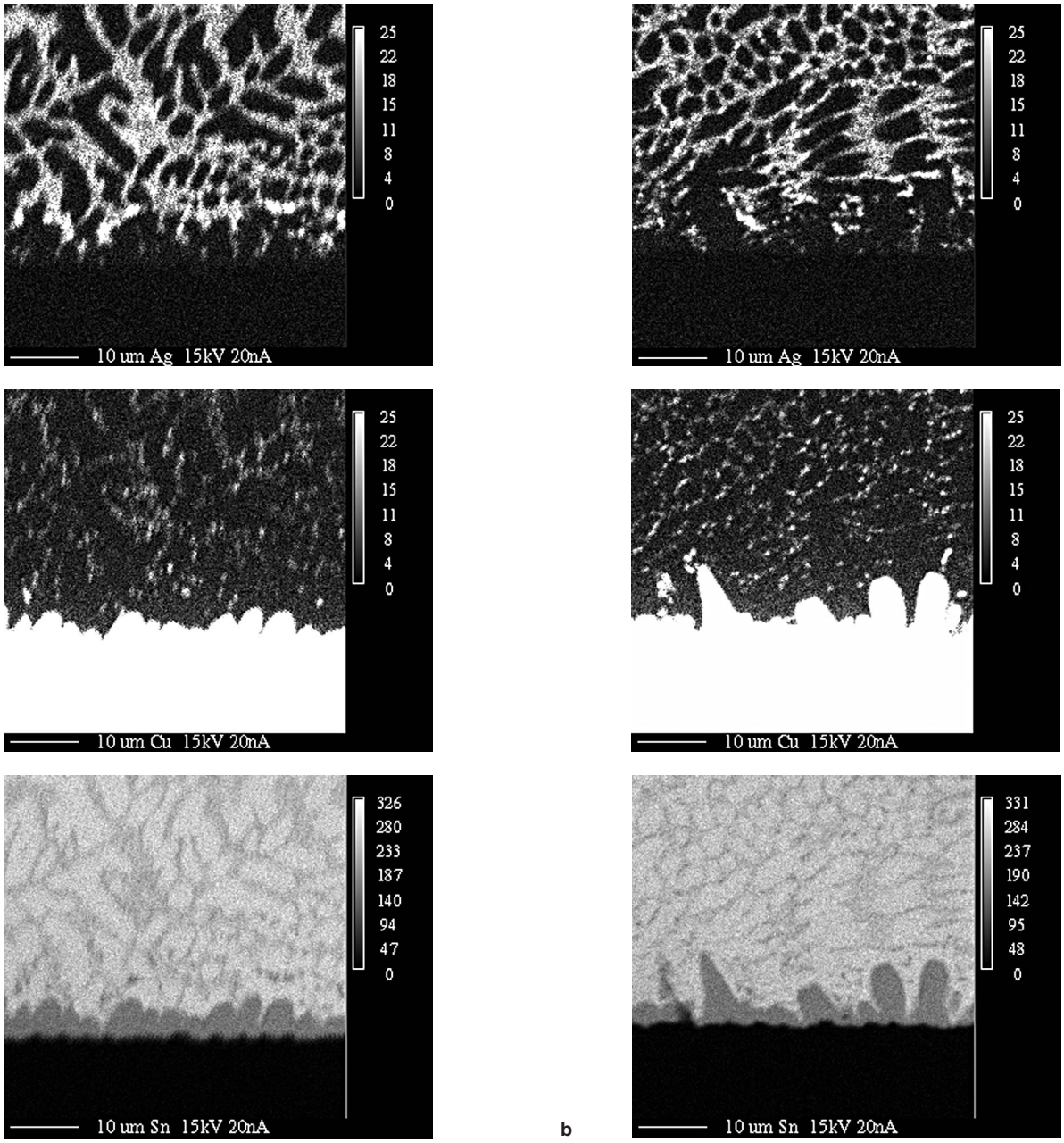

Fig. 9. The EPMA mapping of (a) 0Cu and (b) 1.5Cu on the Cu pad before creep test.

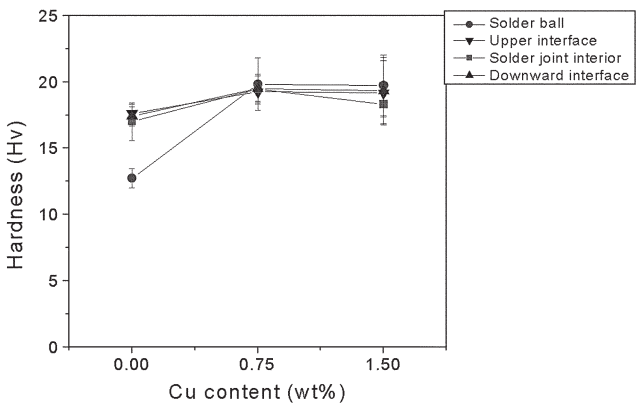

Fig. 10. Vicker's hardness values of each alloy on the Cu pad.

Figure 11 shows the platelike Ag_3Sn IMCs after the 1.5Cu solder was etched away on the Cu pad. Dispersed fine Ag_3Sn particles were found along with the solder matrix in all alloys. These platelike Ag_3Sn was mostly found on the 1.5Cu solder but were rarely found on the 0Cu alloy. This was due to the alloy composition being far from the eutectic point. The interval between the liquidus and solidus line increased, which caused relatively more platelike Ag_3Sn IMCs to form. These large IMC interfaces are very weak because of their incoherence with the matrix. In a real package solder joint, the brittleness of the interphase interface was often observed. It was reported that the crack propagated mostly between the Ag_3Sn intermetallics and β-Sn matrix after thermal cycling.[21]

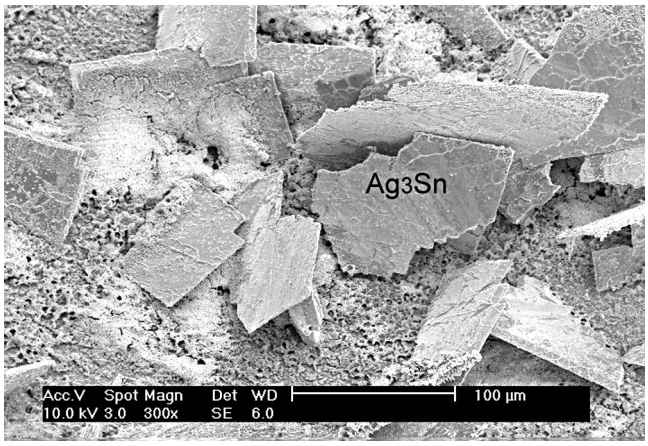

Fig. 11. An SEM image of the Ag_3Sn IMC of which 1.5Cu solder on the Cu pad was etched away.

Interphase sliding was thought to be the main reason for high creep rate in the low stress range. Generally, it is known about grain boundary sliding (GBS) that at high stress, the matrix deformation is faster than GBS, and the effect of GBS is minor. As the stress decreases, substantial GBS occurs and brings a faster creep rate below a certain stress level.[22] From this point of view, high creep rates of the 1.5Cu specimen in the low stress range could be from relatively more platelike Ag_3Sn and coarsened Cu_6Sn_5 IMCs.

Figure 12a is a TEM bright-field image for the 0Cu alloy on the Cu pad. The small particles in the matrix were proved to be Cu_6Sn_5 IMCs. The β-Sn matrix has a tetragonal crystalline structure, as shown in Fig. 12b, and Ag_3Sn has an orthorhombic structure, as shown in Fig. 12c, as the zone axis indicated.

CONCLUSIONS

At the low stress range, creep resistance improved from 7.5Bi, 2.5Bi, 1.5Cu, 0.75Cu, and base alloys on the Cu pad. The Cu-containing alloys were strengthened by the dispersed precipitates of Cu_6Sn_5. Therefore, the Sn-3.5Ag alloy on the Cu pad containing the proper Cu content from the dissolution of Cu showed the best creep resistance. The Cu content increased, while the creep resistance decreased because of the sliding of the interphase interface coming from the relatively more platelike Ag_3Sn and coarsened Cu_6Sn_5 IMCs. The creep properties of the Bi-containing alloy, which showed solid solution strengthening, were not as good as those of the Cu-containing alloy.

ACKNOWLEDGEMENTS

This study was supported by the Center for Electronic Packaging Materials funded by the Korea Science and Engineering Foundation.

REFERENCES

1. S.K. Kang and A.K. Sarkhel, *J. Electron. Mater.* 23, 701 (1994).
2. H. Mavoori, J. Chin, S. Vaynman, B. Moran, L. Keer, and M. Fine, *J. Electron. Mater.* 26, 783 (1997).
3. J. Glazer, *J. Electron. Mater.* 23, 693 (1994).
4. Y. Kariya and M. Otsuka, *J. Electron. Mater.* 27, 1229 (1998).
5. D. Tribula and J.W. Morris, Jr., *ASME Publication* 89-WA/EEP-30 (1989).
6. Z. Mei, D. Grivas, M.C. Shine, and J.W. Morris, Jr., *J. Electron. Mater.* 19, 1273 (1990).
7. J.L. Freer Goldstein and J.W. Morris, Jr., *J. Electron. Mater.* 23, 477 (1994).
8. D. Grivas, K.L. Murty, and J.W. Morris, Jr., *Acta Metall.* 27, 731 (1979).
9. R. Darveaux and K. Banerji, *IEEE Trans. Comp. Hybrids, Manufacturing Technol.* 15, 1013 (1992).
10. M.D. Mathew, S. Movva, H. Yang, and K.L. Murty, *Creep Behavior of Advanced Materials for the 21st Century*, ed. R.S. Mishra, A.K. Murherjee, and K.L. Murty (Warrendale, PA: TMS, 1999), p. 51.
11. S. Wiese, A. Schubert, H. Walter, R. Dudek, F. Feustel, E. Meusel, and B. Michel, *Proc. 51st Electron. Comp. Technol. Conf.* (Piscataway, NJ: IEEE, 2001), pp. 890-902.
12. W.K. Choi and H.M. Lee, *J. Electron. Mater.* 29, 1207 (2000).
13. D.K. Joo, J. Yu, and S.W. Shin, *J. Electron. Mater.* 32, 541 (2003).
14. J. Yu, D.K. Joo, and S.W. Shin, *Acta Mater.* 50, 4315 (2002).
15. J. Cadek, *Creep in Metallic Materials* (New York: Elsevier, 1988), p. 191.

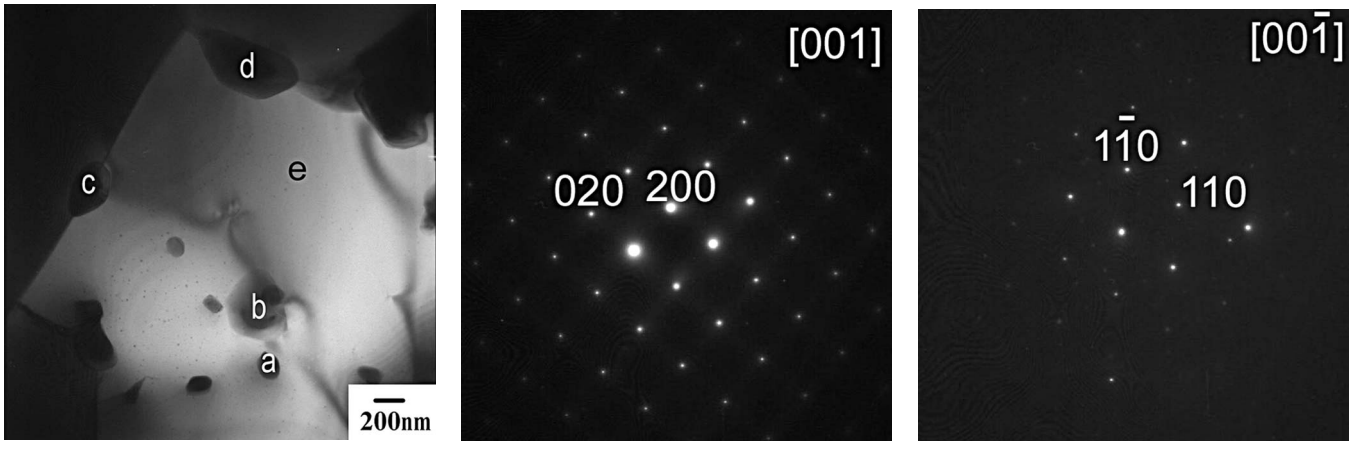

a b c

Fig. 12. (a) A TEM bright-field image for Sn-Ag on a Cu pad; (a) and (b) are Cu_6Sn_5 and (c) and (d) are Ag_3Sn. The selected area diffraction patterns of (b) point e, β-Sn and (c) point d, Ag_3Sn along the zone axis are indicated.

16. Y. Huang and T.G. Langdon, *JOM* 55, 15 (2003).
17. S.W. Shin and J. Yu, *Jpn. J. Appl. Phys.* 42, 1368 (2003).
18. J. Cadek, *Creep in Metallic Materials* (New York: Elsevier, 1988), p. 176.
19. R.J. Mccabe and M.E. Fine, *J. Electron. Mater.* 31, 1276 (2002).
20. M.L. Huang and L. Wang, *J. Mater. Res.* 17, 2897 (2002).
21. A. Schubert, R. Dudek, H. Walter, E. Jung, A. Gollhardt, B. Michel, and H. Reichl, *Proc. 52nd Electronic Components Technology Conf.* (Piscataway, NJ: IEEE, 2002), pp. 1246–1255.
22. W. Beere, *Met. Sci.* 16, 223 (1982).